Electroweak supersymmetry from the generalized minimal supergravity model in the MSSM

Tianjun Li[1,2,*] and Shabbar Raza[1,†]

[1]*State Key Laboratory of Theoretical Physics and Kavli Institute for Theoretical Physics China (KITPC), Institute of Theoretical Physics, Chinese Academy of Sciences, Beijing 100190, People's Republic of China*

[2]*School of Physical Electronics, University of Electronic Science and Technology of China, Chengdu 610054, People's Republic of China*

(Received 22 November 2014; published 16 March 2015)

Considering the generalized minimal supergravity model in the minimal supersymmetric Standard Model, we study the electroweak supersymmetry, in which the squarks and/or gluino are heavy around a few TeVs while the sleptons, sneutrinos, bino, winos, and/or Higgsinos are light within 1 TeV. We resolve the $(g-2)_\mu/2$ discrepancy for the muon anomalous magnetic moment in the Standard Model successfully and identify a parameter space in which such solutions also have the electroweak fine-tuning measures $\Delta_{\rm EW}$ 16.5 (6%) and $\Delta_{\rm EW}$ 25 (4%) without and with the Wilkinson Microwave Anisotropy Probe (WMAP) bounds, respectively. We find that the allowed mass ranges, which are consistent within 3σ of the $g-2$ discrepancy, for the lightest neutralino, charginos, stau, stau neutrinos, and first two-family sleptons are [44, 390], [100, 700], [100, 700], [52, 800], and [150, 800] GeV, respectively. Moreover, our solutions satisfy the latest bounds reported by the ATLAS and CMS collaborations on electroweakinos and sleptons. The colored sparticles such as light stop, gluinos, and the first the first two generations of squark masses have been found in the mass ranges of [500, 3000], [1300, 4300], and [1800, 4200] GeV, respectively. To obtain the observed dark matter relic density for the lightest supersymmetric particle (LSP) neutralino, we have the bino-wino, LSP neutralino-stau, and LSP neutralino-tau sneutrinos coannihilation scenarios and the resonance solutions such as the A pole, Higgs pole, and Z pole. We identify the Higgsino-like LSP neutralino and display its spin-independent and spin-dependent cross sections with nucleons. We present ten benchmark points that can be tested at the up coming collider searches as well.

DOI: 10.1103/PhysRevD.91.055016 PACS numbers: 11.30.Pb

I. INTRODUCTION

It is well known that supersymmetry (SUSY) provides a natural solution to the gauge hierarchy problem in the Standard Model (SM). In the supersymmetric SMs (SSMs), gauge coupling unification can be realized, which strongly indicates the grand unified theories (GUTs), and the electroweak (EW) gauge symmetry can be broken radiatively due to the large top-quark Yukawa coupling. If conservation of R parity is assumed, the lightest supersymmetric particle (LSP) such as a neutralino is a dark matter candidate. Thus, SUSY is the most promising new physics beyond the SM.

From the first run of the LHC, a SM-like Higgs boson with mass m_h around 125 GeV was discovered in July 2012 [1,2]. This is a little bit heavy for the minimal SSM (MSSM) since it requires the multi-TeV top squarks with small mixing or TeV-scale top squarks with large mixing. Moreover, we have strong constraints on the parameter space in the SSMs from the LHC SUSY searches. For example, the gluino mass $m_{\tilde{g}}$ should be heavier than about 1.7 TeV if the first two-generation squark mass $m_{\tilde{q}}$ is around the gluino mass $m_{\tilde{q}} \sim m_{\tilde{g}}$ and heavier than about 1.3 TeV for $m_{\tilde{q}} \gg m_{\tilde{g}}$ [3,4].

Inspired by the LHC Higgs [5] and SUSY [6] searches, as well as the experimental results/constraints on B physics [7,8] and flavor changing neutral current [9–11], anomalous magnetic momentum of the muon [12,13], dark matter relic density from WMAP experiment [14], and direct dark matter search from the LUX experiment [15], one of us (T. L.) with his collaborators proposed electroweak supersymmetry (EWSUSY), in which the squarks and/or gluino are heavy around a few TeVs while the sleptons, sneutrinos, bino, winos, and/or Higgsinos are light within 1 TeV [16]. Especially, the EWSUSY can be realized in generalized minimal supergravity (GmSUGRA) [17,18].

In this paper, we shall systematically study the SM $(g-2)_\mu/2$ discrepancy for the muon anomalous magnetic moment in the MSSM with the EWSUSY from GmSUGRA. We find that the EWSUSY from GmSUGRA not only resolves the $(g-2)_\mu/2$ anomaly but also addresses the electroweak fine-tuning (EWFT) problem. We show the preferred mass ranges for some SUSY-breaking (SSB) terms required to explain the muon $(g-2)_\mu/2$ anomaly. It is well known that neutralinos, charginos (collectively known as electroweakinos), and sleptons play very important roles in addressing the muon $(g-2)_\mu/2$ anomaly. We show that the EWSUSY from

*tli@itp.ac.cn
†shabbar@itp.ac.cn

 © 2015 American Physical Society

GmSUGRA very effectively resolves the muon $(g-2)_\mu/2$ anomaly. The allowed mass ranges consistent within 3σ of the $(g-2)_\mu/2$ discrepancy for the LSP neutralino, charginos, stau, stau neutrinos, and first two families of sleptons are [44, 390], [100, 700], [100, 700], and [52, 800] and [150, 800] GeV, respectively. Recently, the ATLAS and CMS collaborations have reported new bounds on electroweakinos as well as all three families of sleptons and sneutrinos depending on various assumptions and topologies. We discuss these bounds in some detail and find that our solutions are consistent with these bounds and still provide resolution to the muon magnetic dipole moment anomaly within 3σ. We also note that some portions the parameter space are not only consistent with all the collider and astrophysical bounds but also provide even within 1σ contributions to the muon $(g-2)_\mu/2$ and hence resolve the discrepancy successfully. For color sparticles, we note that the light stop is the lightest colored sparticle in our data having mass range [500, 3000] GeV, while gluino mass range is [1300, 4300] GeV. This gluino mass range shrinks a little to 3000 GeV if we insist on dark matter relic density bounds. The first two families of squarks lie in the mass ranges from 1800 to 4200 GeV. We also identify a viable parameter space that satisfies all the bounds including 5σ WMAP9 bounds, resolves the muon $(g-2)_\mu/2$ anomaly, and provides solutions with small EWFT. We note that in our data the minimal EWFT measures $\Delta_{\rm EW} \sim 16.5$ (6%) and $\Delta_{\rm EW} \sim 25$ (4%) without and with the WMAP9 bound, respectively. In our present scans, we find that, in order to obtain the observed dark matter relic density, we have the bino-wino, LSP neutralino-stau, and LSP neutralino-tau sneutrino coannihilation scenarios and resonance solutions such as A resonance, Higgs resonance, and Z resonance for a binolike neutralino. Moreover, we comment on the binolike solutions that do not satisfy the WMAP9 bounds. Apart from the bino-like LSP, we have wino-like and higgsino-like LSPs. These wino-like and higgsino-like LSPs solutions have very small relic density. We comment on such wino-like LSP solutions. We display graphs for direct and indirect searches for higgsino-like LSP. Finally, we present ten benchmark points in two tables showing some characteristic features of our models.

This paper is organized as follows. In Sec. II, we briefly describe the GmSUGRA model and the SSB parameters. We also briefly discuss the $(g_\mu-2)/2$ anomaly and describe our definition of EWFT. In Sec. III, we outline the detailed SSB parameters, the ranges of numerical values employed in our scan, the scanning procedure, and the relevant experimental constraints that we have considered. We discuss results of our scans in Sec. IV. A summary and conclusion are given in Sec. V.

II. EWSUSY FROM THE GMSUGRA IN THE MSSM

In the GmSUGRA [17,18], one can realize the EWSUSY, in which the sleptons and electroweakinos (charginos, bino, wino, and/or Higgsinos) are within 1 TeV while squarks and/or gluinos can be in several TeV mass ranges [16]. Moreover, the gauge coupling relation and gaugino mass relation at the GUT scale are

$$\frac{1}{\alpha_2}-\frac{1}{\alpha_3}=k\left(\frac{1}{\alpha_1}-\frac{1}{\alpha_3}\right), \tag{1}$$

$$\frac{M_2}{\alpha_2}-\frac{M_3}{\alpha_3}=k\left(\frac{M_1}{\alpha_1}-\frac{M_3}{\alpha_3}\right), \tag{2}$$

where k is the index and equal to $5/3$ in the simple GmSUGRA. We obtain a simple gaugino mass relation,

$$M_2-M_3=\frac{5}{3}(M_1-M_3), \tag{3}$$

by assuming gauge coupling unification at the GUT scale ($\alpha_1=\alpha_2=\alpha_3$). It is obvious that the universal gaugino mass relation $M_1=M_2=M_3$ in the mSUGRA is just a special case of this general one. Choosing M_1 and M_2 to be free input parameters, which vary around several hundred GeV for the EWSUSY, we get M_3 from Eq. (3),

$$M_3=\frac{5}{2}M_1-\frac{3}{2}M_2, \tag{4}$$

which could be as large as several TeV or as small as several hundred GeV, depending on specific values of M_1 and M_2.

The general SSB scalar masses at the GUT scale are given in Ref. [18]. Taking the slepton masses as free parameters, we obtain the squark masses in the $SU(5)$ model with an adjoint Higgs field,

$$m^2_{\tilde{Q}_i}=\frac{5}{6}(m_0^U)^2+\frac{1}{6}m^2_{\tilde{E}_i^c}, \tag{5}$$

$$m^2_{\tilde{U}_i^c}=\frac{5}{3}(m_0^U)^2-\frac{2}{3}m^2_{\tilde{E}_i^c}, \tag{6}$$

$$m^2_{\tilde{D}_i^c}=\frac{5}{3}(m_0^U)^2-\frac{2}{3}m^2_{\tilde{L}_i}, \tag{7}$$

where $m_{\tilde{Q}}$, $m_{\tilde{U}^c}$, $m_{\tilde{D}^c}$, $m_{\tilde{L}}$, and $m_{\tilde{E}^c}$ represent the scalar masses of the left-handed squark doublets, right-handed up-type squarks, right-handed down-type squarks, left-handed sleptons, and right-handed sleptons, respectively, while m_0^U is the universal scalar mass, as in the mSUGRA. In the EWSUSY, $m_{\tilde{L}}$ and $m_{\tilde{E}^c}$ are both within 1 TeV, resulting in light sleptons. Especially, in the limit $m_0^U \gg m_{\tilde{L}/\tilde{E}^c}$, we have the approximated relations for squark masses: $2m^2_{\tilde{Q}} \sim m^2_{\tilde{U}^c} \sim m^2_{\tilde{D}^c}$. In addition, the Higgs soft masses $m_{\tilde{H}_u}$ and $m_{\tilde{H}_d}$ and the trilinear soft terms A_U, A_D, and A_E can all be free parameters from the GmSUGRA [16,18].

A. Anomalous magnetic moment of the muon $a_\mu = (g-2)_\mu/2$

In parallel to the ongoing searches for the new physics at the high-energy collider, one can look for such effects at low energy. The precise measurement of muon $a_\mu = (g-2)_\mu/2$ may reveal, though indirectly, traces for the physics beyond the SM. The SM prediction for the anomalous magnetic moment of the muon [12] shows a discrepancy with the experimental results [13], which is quantified as follows:

$$\Delta a_\mu \equiv a_\mu(\text{exp}) - a_\mu(\text{SM}) = (28.6 \pm 8.0) \times 10^{-10}. \quad (8)$$

If SUSY does exist at the EW scale, then the main SUSY contributions to a_μ come from the neutralino-smuon and chargino-sneutrino loops and are given as[1]

$$\Delta a_\mu^{\text{SUSY}} \propto \frac{M_i \mu \tan\beta}{m^4_{\text{SUSY}}}, \quad (9)$$

where $M_i (i = 1, 2)$ are the weak-scale gaugino masses, μ is the Higgsino mass parameter, $\tan\beta \equiv \frac{\langle H_u \rangle}{\langle H_d \rangle}$, and m_{SUSY} is the sparticle mass circulating in the loop. It is also evident from Eq. (9) that, by having appropriately light m_{SUSY} masses (electroweakinos and sleptons), we may have sizable SUSY contributions to Δa_μ. To address the $g-2$ anomaly between experiment and theory, new direct measurements of the muon magnetic moment with fourfold improvement in accuracy have been proposed at Fermilab by the E989 experiment as well as Japan Proton Accelerator Research Complex [20]. First results from E989 are expected around 2017/2018. These measurements will firmly establish or constrain new physics effects. Spurred by these developments, new studies have been done in order to explore this opportunity [16,21]. In this article, while doing general scans, we resolve the muon $(g-2)_\mu/2$ successfully and add new dark matter channels such as Higgs resonance and Z resonance consistent with Δa_μ values within 3σ in addition to the previously reported channels [16,22]. Moreover, we show that our solutions, while having previously mentioned properties, also have small electroweak fine-tuning (defined below). In our scans, the sleptons and electroweakinons mass ranges, which are required to address the $(g-2)_\mu/2$ problem, are in agreement with Refs. [16,22,23].

B. Electroweak fine-tuning

It is interesting to note that, in addition to resolving the a_μ anomaly, the EWSUSY from GmSUGRA can also accommodate the solutions with small EWFT. Upon first glance, it appears contradictory. On one hand, from Eq. (9), it appears that the large values of μ are required for sizable a_μ^{SUSY} contributions. On the other hand, small EWFT requires small values of μ. But after looking at Eq. (9) more carefully, we see that, by having suitable large values for gaugino masses and $\tan\beta$, and small values for electroweakino and slepton masses, one can compensate for the small values of μ (required for small EWFT) and still resolve the a_μ anomaly.

We use the latest (7.84) version of ISAJET [24] to calculate the fine-tuning conditions at the EW scale M_{EW}. After including the one-loop effective potential contributions to the tree-level MSSM Higgs potential, the Z-bosom mass M_Z is given by

$$\frac{M_Z^2}{2} = \frac{(m_{H_d}^2 + \Sigma_d^d) - (m_{H_u}^2 + \Sigma_u^u)\tan^2\beta}{\tan^2\beta - 1} - \mu^2, \quad (10)$$

where Σ_u^u and Σ_d^d are the contributions coming from the one-loop effective potential defined in Ref. [25] and $\tan\beta \equiv \frac{v_u}{v_d}$. All parameters in Eq. (10) are defined at the M_{EW}. To measure the EWFT condition, we follow Ref. [25] and use the definitions

$$\begin{aligned} C_{H_d} &\equiv |m_{H_d}^2/(\tan^2\beta - 1)|, \\ C_{H_u} &\equiv |-m_{H_u}^2 \tan^2\beta/(\tan^2\beta - 1)|, \\ C_\mu &\equiv |-\mu^2|, \end{aligned} \quad (11)$$

with each $C_{\Sigma_{u,d}^{u,d}(k)}$ less than some characteristic value of order M_Z^2. Here, k labels the SM and SUSY particles that contribute to the one-loop Higgs potential. For the fine-tuning measure, we define

$$\Delta_{\text{EW}} \equiv \max(C_k)/(M_Z^2/2). \quad (12)$$

Note that Δ_{EW} only depends on the weak-scale parameters of the SSMs and then is fixed by the particle spectra. Hence, it is independent of how the SUSY particle masses arise. Lower values of Δ_{EW} correspond to less fine-tuning; for example, $\Delta_{\text{EW}} = 10$ implies $\Delta_{\text{EW}}^{-1} = 10\%$ fine-tuning. In addition to Δ_{EW}, ISAJET also calculates Δ_{HS}, which is a measure of fine-tuning at the high scale (HS) like the GUT scale in our case [25]. The HS-scale fine-tuning measure Δ_{HS} is given as follows:

$$\Delta_{\text{HS}} \equiv \max(B_i)/(M_Z^2/2). \quad (13)$$

For the definition of B_i and more details, see Ref. [25].

III. PHENOMENOLOGICAL CONSTRAINTS AND SCANNING PROCEDURE

We employ the ISAJET 7.84 package [24] to perform random scans over the parameter space given below. In this package, the weak-scale values of the gauge and third-generation Yukawa couplings are evolved to M_{GUT} via the

[1]For complete one-loop result, see Ref. [19].

MSSM renormalization group equations (RGEs) in the $\overline{DR}$ regularization scheme. We do not strictly enforce the unification condition $g_3 = g_1 = g_2$ at $M_{\rm GUT}$, since a few percent deviation from unification can be assigned to the unknown GUT-scale threshold corrections [26]. With the boundary conditions given at $M_{\rm GUT}$, all the SSB parameters, along with the gauge and Yukawa couplings, are evolved back to the weak scale M_Z.

In evaluating Yukawa couplings, the SUSY threshold corrections [27] are taken into account at the common scale $M_{\rm SUSY} = \sqrt{m_{\tilde{t}_L} m_{\tilde{t}_R}}$. The entire parameter set is iteratively run between M_Z and $M_{\rm GUT}$ using the full two-loop RGEs until a stable solution is obtained. To better account for the leading-log corrections, one-loop step-beta functions are adopted for gauge and Yukawa couplings, and the SSB parameters m_i are extracted from RGEs at appropriate scales $m_i = m_i(m_i)$. The RGE-improved one-loop effective potential is minimized at an optimized scale $M_{\rm SUSY}$, which effectively accounts for the leading two-loop corrections. The full one-loop radiative corrections are incorporated for all sparticles.

The requirement of radiative electroweak symmetry breaking (REWSB) [28] puts an important theoretical constraint on parameter space. Another important constraint comes from limits on the cosmological abundance of the stable charged particle [29]. This excludes regions in the parameter space in which charged SUSY particles, such as $\tilde{\tau}_1$ or $\tilde{t}_1$, become the LSP. We accept only those solutions for which one of the neutralinos is the LSP.

Using parameters given in Sec. II, we have performed the random scans for the following parameter ranges:

$$\begin{aligned}
100\ \text{GeV} &\le m_0^U \le 5000\ \text{GeV},\\
100\ \text{GeV} &\le M_1 \le 900\ \text{GeV},\\
100\ \text{GeV} &\le M_2 \le 800\ \text{GeV},\\
100\ \text{GeV} &\le m_{\tilde{L}} \le 800\ \text{GeV},\\
100\ \text{GeV} &\le m_{\tilde{E}^c} \le 800\ \text{GeV},\\
100\ \text{GeV} &\le m_{\tilde{H}_{u,d}} \le 5000\ \text{GeV},\\
-6000\ \text{GeV} &\le A_U = A_D \le 5000\ \text{GeV},\\
-800\ \text{GeV} &\le A_E \le 935\ \text{GeV},\\
2 &\le \tan\beta \le 60.
\end{aligned} \tag{14}$$

Also, we consider $\mu > 0$ and use $m_t = 173.3$ GeV [30]. Note that our results are not too sensitive to one or two sigma variation in the value of m_t [31]. We use $m_b^{\overline{DR}}(M_Z) = 2.83$ GeV as well, which is hard coded into ISAJET. Also note that we will use the notations A_t, A_b, and A_τ for A_U, A_D, and A_E, respectively.

In scanning the parameter space, we employ the Metropolis–Hastings algorithm as described in Ref. [32]. The data points collected all satisfy the requirement of REWSB, with the neutralino being the LSP. After collecting the data, we require the following bounds (inspired by the LEP2 experiment) on sparticle masses:

$$m_{\tilde{t}_1}, m_{\tilde{b}_1} \gtrsim 100\ \text{GeV}, \tag{15}$$

$$m_{\tilde{\tau}_1} \gtrsim 105\ \text{GeV}, \tag{16}$$

$$m_{\tilde{\chi}_1^\pm} \gtrsim 103\ \text{GeV}. \tag{17}$$

Moreover, we use the IsaTools package [33,34] and Ref. [35] to implement the following B-physics constraints:

$$0.8 \times 10^{-9} \le \text{BR}(B_s \to \mu^+\mu^-) \le 6.2 \times 10^{-9} (2\sigma) \quad [7], \tag{18}$$

$$2.99 \times 10^{-4} \le \text{BR}(b \to s\gamma) \le 3.87 \times 10^{-4} (2\sigma) \quad [11], \tag{19}$$

$$0.15 \le \frac{\text{BR}(B_u \to \tau\nu_\tau)_{\rm MSSM}}{\text{BR}(B_u \to \tau\nu_\tau)_{\rm SM}} \le 2.41 (3\sigma) \quad [10]. \tag{20}$$

In addition to the above constraints, we impose the following bounds from the LHC and WMAP9 experiments:

$$m_h = 123\text{–}127\ \text{GeV} \quad [1,2], \tag{21}$$

$$m_{\tilde{g}} \gtrsim 1.7\ \text{TeV} \quad (\text{for } m_{\tilde{g}} \sim m_{\tilde{q}}) \quad [3,4], \tag{22}$$

$$m_{\tilde{g}} \gtrsim 1.3\ \text{TeV} \quad (\text{for } m_{\tilde{g}} \ll m_{\tilde{q}}) \quad [3,4], \tag{23}$$

$$0.0913 \le \Omega_{\rm CDM} h^2 (\text{WMAP9}) \le 0.1363 (5\sigma) \quad [14], \tag{24}$$

$$4.7 \times 10^{-10} \le \Delta a_\mu \le 52.7 \times 10^{-10}\ (3\sigma) \quad [13]. \tag{25}$$

IV. NUMERICAL RESULTS

A. Preferred masses required by Δa_μ

In this subsection, we present results of our scans. In Figs. 1 and 2, we present graphs of Δa_μ vs the input parameters given in Sec. III. In these plots, grey points (grey in black and white print) satisfy the REWSB and LSP neutralino conditions, aqua points (slightly dark grey in black and white print) satisfy the mass bounds, B-physics bounds, and 123 GeV $\le m_h \le$ 127 GeV, and red points (dark grey in black and white print) are subset of aqua points that also satisfy the WMAP9 5σ bounds. In Fig. 1, we display graphs in the $M_1 - \Delta a_\mu$, $M_2 - \Delta a_\mu$, $M_3 - \Delta a_\mu$, $A_t(= A_b) - \Delta a_\mu$, $A_\tau - \Delta a_\mu$, and $\tan\beta - \Delta a_\mu$ planes. At first, we did general scans over the parameter space given by Eq. (14), and then we did the dedicate scans around the phenomenologically interesting solutions. These dedicated searches appear as patches in the graphs. In the top left panel, we see that aqua points have M_1 mass range [100, 900] GeV, which also have 3σ to 1σ contributions to Δa_μ. There is a lack of gray points between

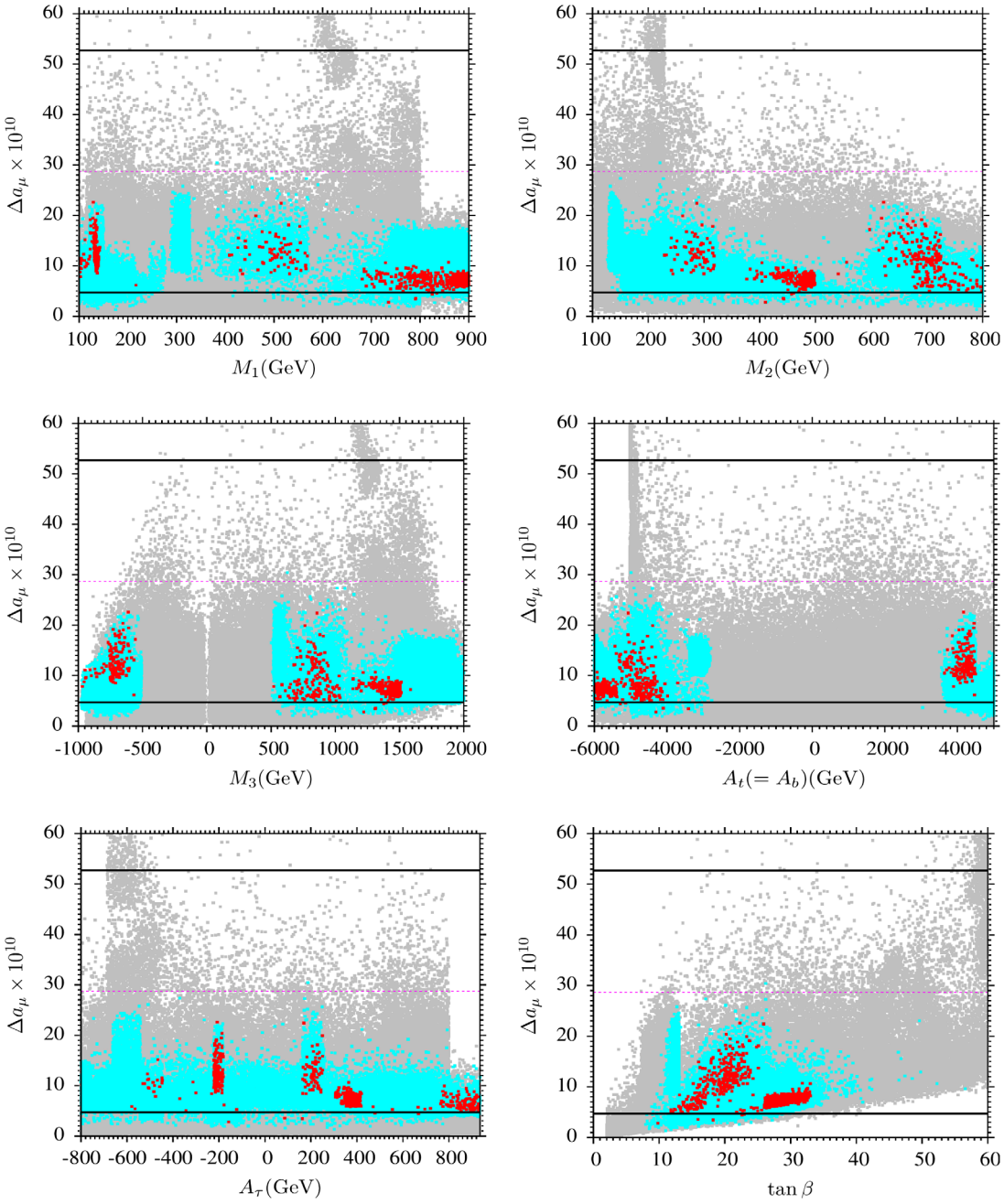

FIG. 1 (color online). Plots in $M_1 - \Delta a_\mu$, $M_2 - \Delta a_\mu$, $M_3 - \Delta a_\mu$, $A_t(= A_b) - \Delta a_\mu$, $A_\tau - \Delta a_\mu$, and $\tan\beta - \Delta a_\mu$. Grey points (grey in black and white print) satisfy the REWSB and LSP neutralino conditions. Aqua points (slightly grey in black and white print) satisfy the mass bounds, B-physics bounds and 123 GeV $\leq m_h \leq$ 127 GeV. Red points (dark grey in black and white print) are subset of aqua points that also satisfy the WMAP9 5σ bounds. The horizontal black solid lines represent 3σ Δa_μ values, and the dashed purple lines show the central value of Δa_μ.

800 GeV $\lesssim M_1 \lesssim$ 900 GeV. It is because initially we generated data up to $M_1 = 800$ GeV. To get the light CP-even Higgs boson mass around 125 GeV, we then did some dedicated searches in which we had to increase upper ranges of a couple of input parameters. This is the reason why one can see the sharp cut in gray points in this plot and plots in the $A_t(= A_b) - \Delta a_\mu$ and $A_\tau - \Delta a_\mu$ planes. Another point to be noted is that we do not see any preferred range of M_1 to have large contribution to Δa_μ. Apparently, there are more points between 400 GeV $\lesssim M_1 \lesssim$ 800 GeV where we see large values for Δa_μ. But in fact, by generating more data, it can be shown that we have more or less the same contributions to Δa_μ for all values of M_1 between [100, 900] GeV. Since our parameter space is very large, doing these kind of scans is a very time-consuming job. But the main purpose of this study is to show that the

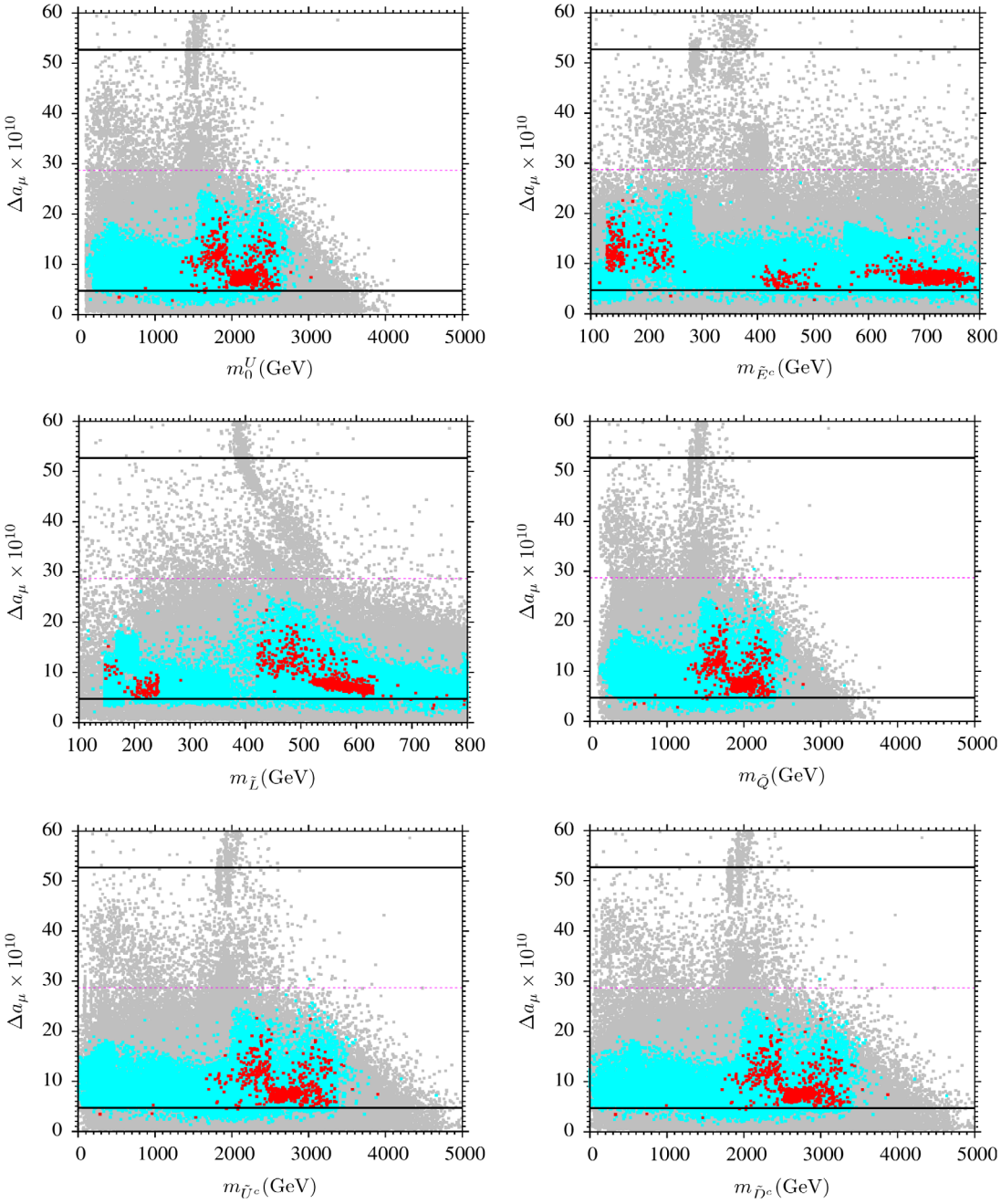

FIG. 2 (color online). Plots in the $m_0^U - \Delta a_\mu$, $m_E - \Delta a_\mu$, $m_L - \Delta a_\mu$, $m_Q - \Delta a_\mu$, $m_U - \Delta a_\mu$, and $m_D - \Delta a_\mu$ planes. The color coding is the same as in Fig. 1.

EWSUSY from GmSUGRA can resolve the apparent discrepancy of muon Δa_μ, which is clearly displayed. Moreover, we find that even red points can have any value of M_1 between [100, 900] GeV. We note that red points with small M_1 values ($M_1 \lesssim 150$ GeV) with 2σ contributions to Δa_μ represent resonance solutions like the Z pole and Higgs pole. We will discuss such a solution in Sec. IV D. We also see that in our present data with $M_1 \sim$ 500 GeV red points have contributions to Δa_μ within 1σ. In the top right panel, we note that aqua points can have M_2 values between 140 and 800 GeV and within 3σ bounds of Δa_μ. The small values of M_2 indicate the presence of a light wino-type LSP neutralino. On the other hand, the minimal and maximal M_2 values for red points are between 250 and 800 GeV. In the middle left panel, we display values for M_3 that we calculate using Eq. (4). Here, one can see that we have solutions with both $M_3 < 0$ and $M_3 > 0$. To have 3σ or better Δa_μ contributions and remain consistent with the constraints discussed in Sec. III, we need in both cases $|M_3| > 500$ GeV, which indicates a relatively heavy gluino. The right middle panel depicts that in our model with $|A_t| = |A_b| > 3000$ GeV, we have the sizable SUSY

contribution to Δa_μ and consistent with the bounds given in Sec. III. These relatively large values of $|A_t|$ will also help to get the Higgs boson mass around 125 GeV. In the left bottom panel, we observe that aqua solutions have A_τ range anywhere between -800 GeV $\lesssim A_\tau \lesssim 935$ GeV. But for red points, we have -600 GeV $\lesssim A_\tau \lesssim 935$ GeV. In the bottom right panel, we see that the contributions to Δa_μ increase as $\tan\beta$ increases, which can be understood from Eq. (9). For $\tan\beta \approx 12$–50 and 20–25, respectively, for aqua and red points, we have solutions within 1σ $(20.7 \times 10^{-10} - 36.7 \times 10^{-10})$ bounds on Δa_μ. As we discussed earlier, the large $\tan\beta$ along with large μ values may help to get the desired Δa_μ values. But the large left-right stau mixing term A_τ may generate the electric charge breaking minimum in the scalar potential as indicated in Ref. [36]. It was shown in Ref. [37] that one can have a metastability condition for the electric charge breaking in terms of μ, $\tan\beta$, $m_{\tilde{\tau}_L}$, and $m_{\tilde{\tau}_R}$ (also see Ref. [38]), in which the product $\mu\tan\beta$ should be less than some combination of $m_{\tilde{\tau}_L}$ and $m_{\tilde{\tau}_R}$. Although in our case we do not have the very large A_τ values, we still use Eq. (11) of Ref. [37] to filter out points that do not satisfy the metastability condition.

In Fig. 2, we show plots in the $m_0^U - \Delta a_\mu$, $m_{\tilde{E}^c} - \Delta a_\mu$, $m_{\tilde{L}} - \Delta a_\mu$, $m_{\tilde{Q}} - \Delta a_\mu$, $m_{\tilde{U}^c} - \Delta a_\mu$, and $m_{\tilde{D}^c} - \Delta a_\mu$ planes. The color coding is the same as in Fig. 1. In top left panel, we see that m_0^U is anywhere between 100 and 3600 GeV if we consider aqua points, but for red points, it is restricted to be around 3000 GeV. In the right top panel, we observe that aqua points within 1–3σ bounds on Δa_μ have m_{E^c} from 100 to 800 GeV. Similarly, red points share the same mass range. The middle left plot shows the mass range [130, 800] GeV for the universal left-handed sleptons $\tilde{L}$. Like the right-handed sleptons, $\tilde{E}^c$ and $\tilde{L}$ more or less share the same mass range for both aqua and red points. In the right middle, bottom left, and bottom right panels, we display masses for left-handed, right-handed up-type, and down-type squarks, respectively, which we calculate by using Eq. (7). For the left-handed squarks, we have slightly narrow allowed mass ranges as compared to the right-handed squarks. Also, $\tilde{U}^c$ and $\tilde{D}^c$ have almost the same mass ranges, which are consistent with Eq. (7).

B. Compatibility between the Δa_μ bound and EWFT

Figure 3 displays plots in the $m_h - \Delta a_\mu$, $\Delta_{\rm EW} - \Delta a_\mu$, and $\Delta_{\rm EW} - \Delta a_\mu$ planes. The color coding is the same as in Fig. 1 except that in the $m_h - \Delta a_\mu$ plane we do not apply Higgs mass bound. The left panel shows plenty of solutions accommodating bounds on Higgs boson mass 123–127 GeV, having sizable contributions to Δa_μ and being consistent

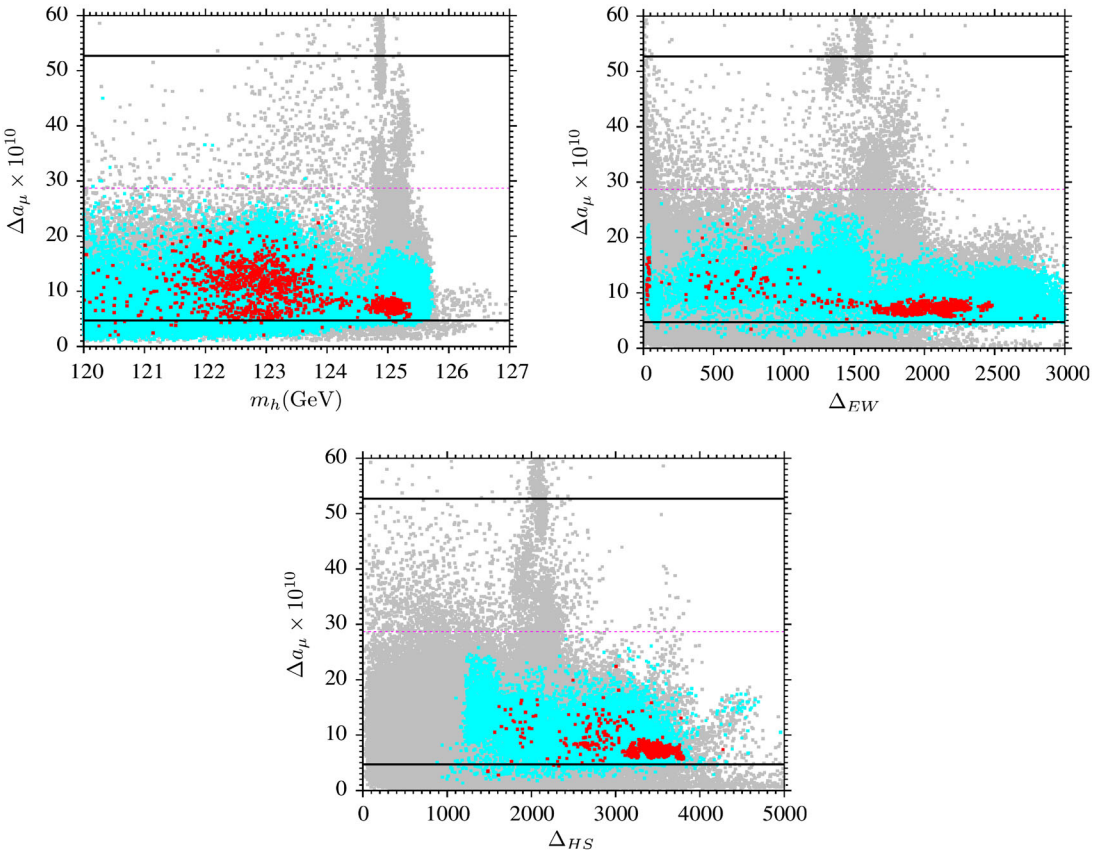

FIG. 3 (color online). Plots in the $m_h - \Delta a_\mu$, $\Delta_{\rm EW} - \Delta a_\mu$, and $\Delta_{\rm HS} - \Delta a_\mu$ planes. The color coding is the same as in Fig. 1 except that in the $m_h - \Delta a_\mu$ plane we do not apply the Higgs boson mass bound.

with the sparticle mass bounds and B-physics bounds mentioned in Sec. III. Red points are mostly concentrated in the Higgs boson mass range 123 GeV $\lesssim m_h \lesssim$ 124 GeV and have Δa_μ contributions within 2σ. In the left panel, we find that aqua and red points have small values for fine-tuning measure $\Delta_{\rm EW}$. These points not only resolve the Δa_μ discrepancy but also provide a solution to the EWFT problem. As we mentioned earlier, this can be understood from Eq. (9), where we see that the SUSY contribution to Δa_μ is proportional to μ, gaugino masses ($M_{1,2}$), and $\tan\beta$ but inversely proportional to the fourth power of $m_{\rm SUSY}$ (the mass scale related to charginos, smuons, sneutrino, and neutralinos). Small EWFT requires small values of μ, while sizable Δa_μ contributions have the opposite requirement for μ. But if the gaugino masses and $\tan\beta$ are appropriately large (as can be seen in Fig. 1) and $m_{\rm SUSY}$ is small (as can be seen below in Fig. 4), one can indeed have sizable Δa_μ. In our data, the minimal value of $\Delta_{\rm EW}$ is about 16.5 (6%) with $\Delta a_\mu \approx 11.6 \times 10^{-10}$ for aqua points, and for red points, $\Delta_{\rm EW}$ can be as small as 25 (4%) with $\Delta a_\mu \approx 15.1 \times 10^{-10}$. A plot in $\Delta_{\rm HS} - \Delta a_\mu$ is also shown for the comparison of $g-2$ with the HS fine-tuning measure. Here, it can be seen that the points, which have low $\Delta_{\rm HS}$ values, have relatively large Δa_μ values and vice versa.

C. Supersymmetry searches at the LHC

The viable parameter space in the SSMs is still large, so efforts are going on to find its evidence(s). If R parity is conserved, SUSY particles are pair produced, and the lightest neutralino in most of the cases is the LSP and thus dark matter candidate. Charginos ($\tilde\chi^\pm_{1,2,}$) and neutralinos ($\tilde\chi^0_{1,2,3,4}$) can decay into leptonic final states via superpartners of neutrinos ($\tilde\nu$, sneutrinos) or charged leptons ($\tilde l$, sleptons), or via W, Z, or Higgs (h) bosons ($\tilde\chi^\pm_i \to \ell^\pm\tilde\nu, \nu\tilde\ell^\pm, W^\pm\tilde\chi^0_j, Z\tilde\chi^\pm_j, h\tilde\chi^\pm_j$ and $\tilde\chi^0_i \to \nu\tilde\nu, \ell^\pm\tilde\ell^\mp, W^\pm\tilde\chi^\mp_j, Z\tilde\chi^0_j, h\tilde\chi^0_j$, respectively). In recent studies, the ATLAS and CMS collaborations have reported new bounds on electroweakinos. For example, in Ref. [39], direct production of charginos and neutralinos is presented in events with three leptons and missing transverse energy $E_T^{\rm miss}$ for 8 TeV center-of-mass energy. Here, the simplified models are employed to study the direct pair production of $\tilde\chi^\pm_1$ and $\tilde\chi^0_2$. $\tilde\chi^\pm_1$ and $\tilde\chi^0_2$ are assumed to be degenerate and consist purely of a wino component. In this study, $\tilde\chi^0_1$ is assumed to be pure bino.[2] In such scenarios, if $\tilde\chi^\pm_1$ and $\tilde\chi^0_2$ decay via the first two-generation sleptons and sneutrinos $\tilde l/\tilde\nu$, their masses can be excluded up to 700 GeV. On the other hand, if only $\tilde\tau/\tilde\nu_\tau$ as the next-to-LSP (NLSP) are involved while the first two generations of sleptons/sneutrinos are heavy, then the lower mass limit for $\tilde\chi^\pm_1$ and $\tilde\chi^0_2$ is 380 GeV. In the case of W/Z and W/h mediated decays, $\tilde\chi^\pm_1$ and $\tilde\chi^0_2$ mass limits are 345 and 148 GeV respectively. In another ATLAS SUSY searche [40], the direct productions of charginos, neutralinos, and sleptons in the final states with two leptons and missing transverse energy at 8 TeV center-of-mass energy is reported. Here, too, $\tilde\chi^\pm_1$ and $\tilde\chi^0_2$ are assumed to be degenerate and pure winos while $\tilde\chi^0_1$ is pure bino. In the scenario in which the masses of sleptons and sneutrinos lie between $\tilde\chi^\pm_1$ and $\tilde\chi^0_1$, $\tilde\chi^\pm_1$ decays promptly to $l\nu\tilde\chi^0_1$ via $\tilde l\nu$ or $l^\pm\tilde\nu$, and its mass can be excluded in the range [140, 465] GeV. On the other hand, if $\tilde\chi^\pm_1$ is the NLSP and decays via W to $l\nu\tilde\chi^0_1$, its mass is excluded in the ranges [100, 105], [120, 135], and [145, 160] GeV. In another scenario, $\tilde\chi^\pm_1$ and $\tilde\chi^0_2$ are considered mass degenerate and NLSPs, the direct $\tilde\chi^\pm_1\tilde\chi^0_2$ pair-production is followed by the decays $\tilde\chi^\pm_1 \to W^\pm\tilde\chi^0_1$ with a 100% branching fraction. In this case, the excluded mass range for $\tilde\chi^\pm_1$ and $\tilde\chi^0_2$ is [180, 335] GeV. In a scenario in which slepton $\tilde l$ is the NLSP ($pp \to \tilde l^+\tilde l^- \to l^\pm\tilde\chi^0_1$), the common values of the left- and right-handed selectron and smuons masses between 90 and 325 GeV are excluded, and for $m_{\tilde\chi^0_1} = 100$ GeV, the common values of the left- and right-handed slectron and smuons masses between 160 and 310 GeV are excluded. Similar studies have also been reported by the CMS Collaboration [41]. In light of these results, we investigate our data in Fig. 4. The color coding for this figure is the following. Blue points (black points in black and white print) represent the bino-type LSP neutralino, satisfy REWSB, and are consistent with the bounds on sparticle/Higgs masses including 123 GeV $\le m_h \le$ 127 GeV, B-physics, and $4.7 \times 10^{-10} \lesssim \Delta a_\mu \lesssim 52.7 \times 10^{-10}$. Red points (dark grey points in black and white print) are a subset of that blue points that satisfy the WMAP9 5σ bounds. The black solid lines are just to guide the eyes where we expect mass degeneracy in LSP neutralino and other sparticle masses. We present the plot in the $m_{\tilde\chi^\pm_1} - m_{\tilde\chi^0_1}$ plane in the left top panel. Here, blue and red points along the line represent the bino-wino coannihilation solutions. The chargino mass ranges for these points are [140, 410] and ~[180, 410] GeV for blue and red points, respectively. Interestingly, these red solutions are consistent with the bounds on the NLSP $\tilde\chi^\pm_1$ mentioned above. There is a horizontal strip of points along $m_{\tilde\chi^0_1} \approx 45$ GeV, which are the Z-pole solutions. We also have another horizontal strip of red points around $m_{\tilde\chi^\pm_1} \sim 430$ and $m_{\tilde\chi^0_1} \sim 60$ GeV that represents Higgs-pole solutions. The above-mentioned bounds on charginos do not apply on the resonance solutions. We will discuss these solutions later on. We also find blue and red points with $m_{\tilde\chi^0_1} \gtrsim 150$ GeV and 100 GeV $\lesssim m_{\tilde\chi^\pm_1} \lesssim 700$ GeV. These are the points where the NLSPs are sleptons or sneutrinos (either the first two generations or third generation). We

[2]In the results given below, $m_{\tilde\chi^0_1} = 0$ is assumed unless stated otherwise.

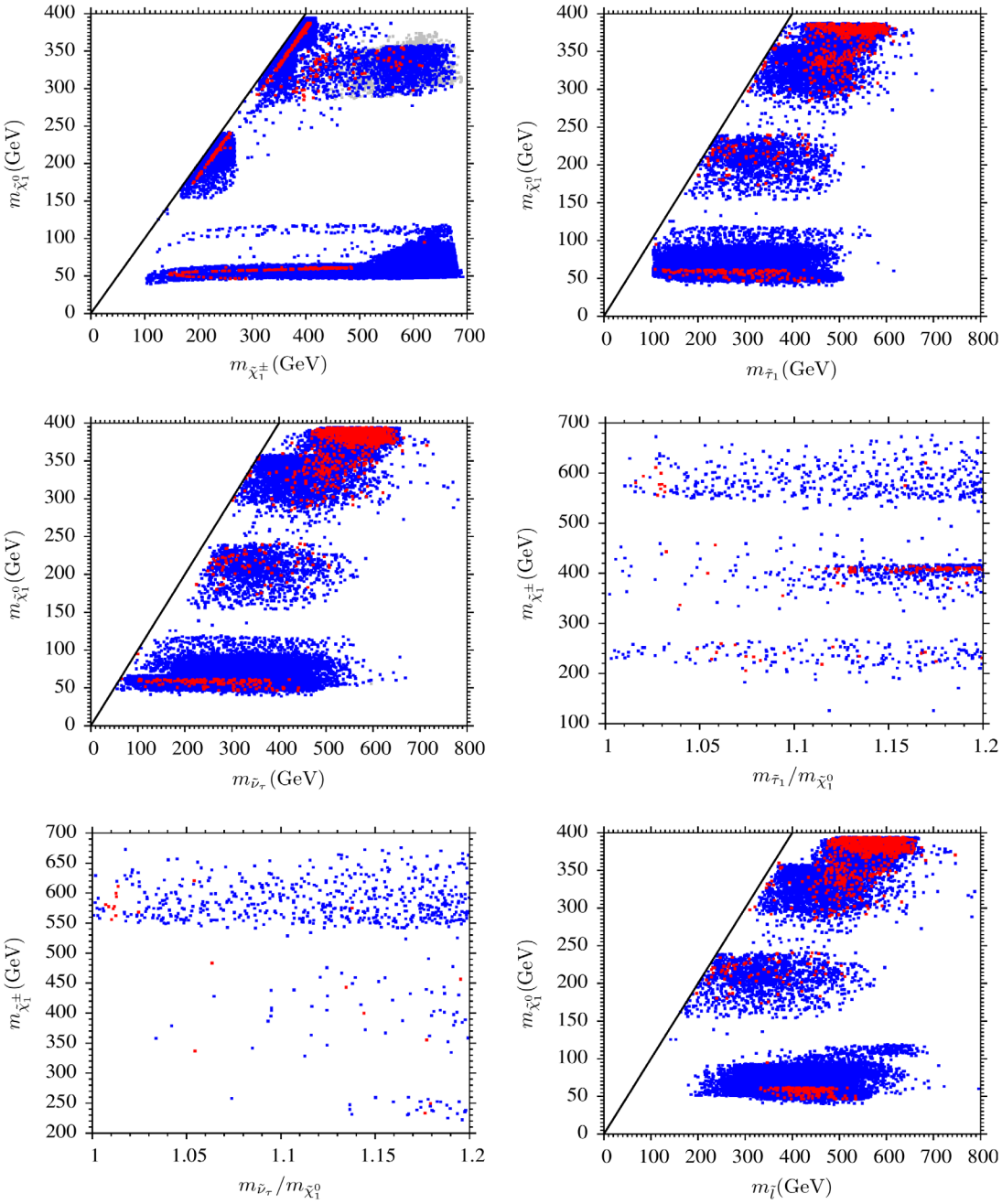

FIG. 4 (color online). Plots in the $m_{\tilde{\chi}_1^\pm} - m_{\tilde{\chi}_1^0}$, $m_{\tilde{\tau}_1} - m_{\tilde{\chi}_1^0}$, $m_{\tilde{\nu}_\tau} - m_{\tilde{\chi}_1^0}$, $m_{\tilde{\tau}_1}/m_{\tilde{\chi}_1^0} - m_{\tilde{\chi}_1^\pm}$, $m_{\tilde{\nu}_\tau}/m_{\tilde{\chi}_1^0} - m_{\tilde{\chi}_1^\pm}$, and $m_{\tilde{l}} - m_{\tilde{\chi}_1^0}$ planes. Blue points (black points in black and white print) represent the bino-type LSP neutralino and satisfy REWSB. They are consistent with bounds on sparticle and Higgs boson masses including 123 GeV $\leq m_h \leq$ 127 GeV, B-physics, and $4.7 \times 10^{-10} \lesssim \Delta a_\mu \lesssim 52.7 \times 10^{-10}$. Red points (dark grey points in black and white print) are subset of blue points that satisfy the WMAP9 5σ bound.

have to be careful about all of these points and check their status. For this purpose, we display plots in the $m_{\tilde{\tau}_1} - m_{\tilde{\chi}_1^0}$ and $m_{\tilde{\nu}_\tau} - m_{\tilde{\chi}_1^0}$ planes. In these plots, there are points where the stau and tau sneutrino are the NLSPs and are degenerate in mass with the LSP neutralino. To make sure whether these NLSP solutions satisfy the bounds on charginos discussed above, we present plots in the $m_{\tilde{\tau}_1}/m_{\tilde{\chi}_1^0} - m_{\tilde{\chi}_1^\pm}$ and $m_{\tilde{\nu}_\tau}/m_{\tilde{\chi}_1^0} - m_{\tilde{\chi}_1^\pm}$ planes. These plots clearly show that all the points $m_{\tilde{\chi}_1^\pm} \gtrsim 380$ GeV are allowed as they satisfy the chargino mass bounds in the case of $\tilde{\tau}/\tilde{\nu}_\tau$-mediated chargino decays given above. In the bottom left panel, we display the plot in the $m_{\tilde{l}} - m_{\tilde{\chi}_1^0}$ plane, which shows that most of our solutions easily satisfy the upper bounds on the first two-generation slepton masses 325 and 310 GeV, respectively, for $m_{\tilde{\chi}_1^0} = 0$ and 150 GeV.

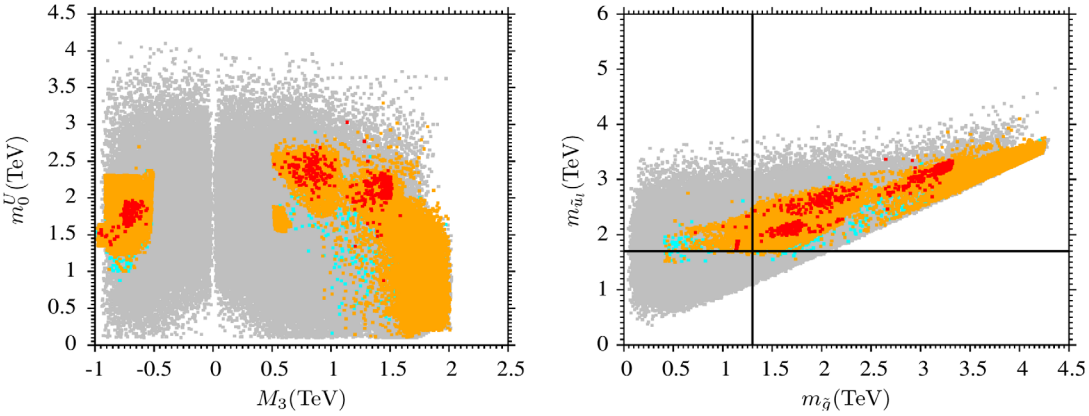

FIG. 5 (color online). Plots in the $M_3 - m_0^U$ and $m_{\tilde{g}} - m_{\tilde{u}_l}$ planes. Gray points satisfy the REWSB and the lightest neutralino as LSP conditions. Aqua points (slightly dark grey points in black and white print) satisfy the sparticle mass bounds, B-physics bounds, and 123 GeV $\leq m_h \leq$ 127 GeV. Orange points (slightly dark grey points in black and white print) form a subset of aqua points which satisfy the 3σ bounds on Δa_μ. Red points (dark grey points in black and white print) are a subset of orange points that also satisfy the WMAP9 5σ bounds. Also, we do not apply the squark and gluino mass bounds on the right panel, which are 1.8 and 1.3 TeV, respectively.

In Fig. 5, we present plots in the $M_3 - m_0^U$ and $m_{\tilde{g}} - m_{\tilde{u}_l}$ planes. Gray points satisfy the REWSB and neutralino as LSP conditions. Aqua points satisfy the mass bounds, B-physics bounds, and 123 GeV $\leq m_h \leq$ 127 GeV. Orange points form a subset of aqua points that satisfy the 3σ bounds on Δa_μ. Red points are a subset of orange points that also satisfy WMAP9 5σ bounds. In the left panel, orange points can be divided in three portions. In the case of large M_3 and large m_0^U, all colored sparticles are decoupled with masses around several TeV. For large M_3 and small m_0^U, the colored sparticle spectra will be similar. However, when M_3 is small but m_0^U is large, the gluino is light around or below 1 TeV, while squarks are heavy. The mass squared (mass^2) of the right-handed squarks is predicted to be approximately twice the left-handed ones. In the right panel, we show the mass ranges for the gluino and left-handed squarks in our scans and do not apply squark and gluino mass bounds here. The black horizontal and vertical lines represent the squark and gluino bounds. For orange points, the gluino mass range is about $\sim$[1300, 4300] GeV, corresponding to squark mass range $\sim$[1800, 4000] GeV. While for red points, the upper limits on gluino and squark masses are relatively light about 3400 GeV. Here, we also note that, because we have relatively light gluinos compared to $m_{\tilde{g}} \gtrsim 2$ TeV reported in Refs. [16,22], our parameter space can be probed easily at the next round of LHC supersymmetry searches. It is shown in Ref. [42] that the squarks and gluino with masses around 2.5, 3, and 6 TeV may be probed by the LHC14, high-luminosity LHC14, and high-energy LHC33, respectively. This clearly shows that our models have testable predictions. Moreover, if we have a collider facility with even higher energy in the future, we will be able to probe even larger values of sparticle masses.

D. Dark matter relic density

In this subsection, we discuss the possible mechanism through which in our present scans we get the observed dark matter relic density and also satisfy all the phenomenological bounds such as sparticle mass bounds, the Higgs boson mass bounds, 3σ bounds on Δa_μ, and B-physics bounds. We have already shown the existence of the bino-wino coannihilation scenario in our model in the top left panel of Fig. 4. Just to remind the reader, red points in that figure satisfy all the bounds just mentioned above. We see red points along the black line with chargino mass 170–410 GeV. Some portions of this mass range have already been explored by the LHC searches as discussed above. The International Linear Collider (ILC), a proposed e^+e^- collider [43,44], was designed to operate at center-of-mass energy $\sqrt{s} \sim 0.25$–1 TeV. At the ILC, one can probe the chargino mass up to $\sqrt{s}/2$. This clearly shows that the entire chrgino mass range mentioned above can be tested at the ILC, and we can have valuable information about SUSY contributions to $g-2$ indirectly. Moreover, in the same plot, we can see the Z-pole solutions with $m_{\tilde{\chi}_1^0} \sim 45$ GeV. Such solutions are constrained by the decay width of Z-boson to a pair of dark matter particles, $\Delta\Gamma(Z \to \chi_1^0\chi_1^0) < 0.2$ [45]. It was shown in Ref. [46] that this decay width can be translated for the bino-LSP case in terms of μ and $\mu \gtrsim 140$ GeV is required in order to avoid the experimental bound. We have checked that all of our red points satisfy this bound.

In the same plane, there exist the Higgs-resonance solutions as a horizontal strip of red points around $m_{\tilde{\chi}_1^0} \sim 60$ GeV. We show ooint 1 in Table II as an example of such solutions. In particular, note that Br(higgs $\to \tilde{\chi}_1^0\tilde{\chi}_1^0$) $\sim 4.68 \times 10^{-4}$, which is consistent with the results

reported in Ref. [47]. In the top right and middle left panels of Fig. 4, it is easy to see that we can accommodate the LSP neutralino-stau and LSP neutralino-tau sneutrino coannihilation scenarios. The middle right and bottom left panels of Fig. 4 show that in these scenarios solutions with $\tilde{\chi}_1^{\pm} \gtrsim 380$ GeV do survive. Because the production cross section of $\tilde{\chi}_1^{\pm}\tilde{\chi}_2^0$ is very large as compared to sleptons, it will be very hard to probe such solutions at the LHC. Apart from Higgs-pole and Z-pole solutions, we also have A-resonance solutions, as can be seen in Fig. 6. The color coding is the same as in Fig. 4, and the black line there represents $m_A = 2m_{\tilde{\chi}_1^0}$. For blue points, we have m_A as light as 370 GeV and as heavy as 700 GeV along the line. While for red points, the lower limit for m_A is about 600 GeV. Apart from our red points that satisfy the 5σ WMAP9 bound in Figs. 4 and 6, we would like to comment on blue points. These blue solutions have Ωh^2 values either above or below the 5σ WMAP9 bounds. To solve this problem, in the former case, one can treat the bino as the NLSP and assume that it decays to a lighter state, for example, $\tilde{\chi}_1^0 \to \gamma\tilde{a}$, where $\tilde{a}$ is an axino. In such a scenario, we will have the mixed axion and axino ($a\tilde{a}$) dark matter [48]. In the latter case in which we have relic density $\Omega h^2 \sim 10^{-5} - 10^{-2}$, the neutralino abundance can be accommodated in the Pecci–Quinn augmented MSSM, where $m_{\tilde{a}} > m_{\tilde{\chi}_1^0}$ and additional neutralinos are produced via thermal axino production and decay $m_{\tilde{a}} \to m_{\tilde{\chi}_1^0}\gamma$ [49]. In these cases, the cold dark matter tends to be neutralino dominant with a small component of axions. In addition to the bino-type neutralino LSP, we have the wino-type and Higgsino-type neutralino LSPs as well. Let us discuss them one by one. It was shown in Refs. [50,51] that for Navarro-Frenk-White and Einasto distributions the entire mass range of thermal wino dark matter from 0.1 to 3 TeV may be excluded. In a recent study [52], it was shown that the wino as a dark matter candidate is excluded in the mass range below 800 GeV from the antiproton and between 1.8 and 3.5 TeV from the absence of a γ-ray line feature toward the Galactic center. Because our wino-type solutions have very small relic density from 10^{-3} to 10^{-5}, for example, point 5 in Table I, the light winolike LSP neutralino, which can provide a solution to the a_μ anomaly, does satisfy the above constraints. Even if one has a thermal winolike LSP neutralino with mass around 2.8 TeV and the observed relic density, one can escape the above bounds by assuming that the winolike neutralino is the NLSP and decays to an axino and γ. Another example of solutions with under abundance relic density is the Higgsino-like LSP. To match the observed dark matter relic density, we need an additional dark matter candidate along with a Higgsino. In this scenario, the Higgsino could make only a small fraction of the dark matter relic density, and the remaining abundance is composed of axinos produced through the vacuum misalignment [53]. This also provides the possibility to detect axinos along with the chances to detect Higgsinos despite the fact that their relic density is somewhat suppressed between 1 and 15 in the present Universe. In the top left panel of Fig. 7, we plot the rescaled Higgsino-like neutralino spin-independent cross section $\xi\sigma^{\rm SI}(\tilde{\chi}_1^0 p)$ vs m(Higgsino). The orange solid line (top greyish solid line in black and white print) represents the current upper bound set by the CDMS experiment, the black solid line depicts the upper bound set by the XENON100 experiment [54], and the current upper bound set by the LUX experiment [15] is shown by purple line (greyish solid line in black and white print), while the orange (greyish in black and white print) and black dashed lines represent, respectively, the future reach of the SuperCDMS [55] and XENON1T [56] experiments. To account for the fact that the local Higgsino relic density might be much less than the usually assumed value $\rho_{\rm local} \simeq 0.3$ GeV/cm^3, we rescale our results by a factor $\xi = \Omega_{\tilde{\chi}_1^0}h^2/0.11$ [57]. Blue points satisfy all the bounds mentioned in Sec. III except the WMAP9 bounds. We note that these solutions have $50 \lesssim \Delta_{\rm EW} \lesssim 130$ and most of the solutions have $\Delta_{\rm EW} \lesssim 100$. However, the solutions with m(Higgsino) in the range [100, 325] GeV can be ruled out by the LUX experiment depending upon their $\xi\sigma^{\rm SI}(\tilde{\chi}_1^0 p)$ values. The rest of the solutions with small values of $\xi\sigma^{\rm SI}(\tilde{\chi}_1^0 p)$ will be probed by the SuperCDMS and XENON1T experiments, but not completely. Here, we would like to comment on our solutions just below the XENON1T reach line with Higgsino mass around m(Higgsino) $\sim$ 200 and 300 GeV, which have $\mu \sim$ 209 and 313 GeV, while $\Delta_{\rm EW} \sim$ 102 and 128, respectively. The presence of this point shows that it would be difficult to rule out the Higgsino-like LSP neutralino for entire parameter space in R-parity conserving natural SUSY models [58]. The top right panel shows a plot in the rescaled Higgsino-like neutralino spin-dependent cross section $\xi\sigma^{\rm SD}(\tilde{\chi}_1^0 p)$ as a function of m(Higgsino). The green line represents the upper bound set by the COUPP experiment [59]. We see that our solutions are about a

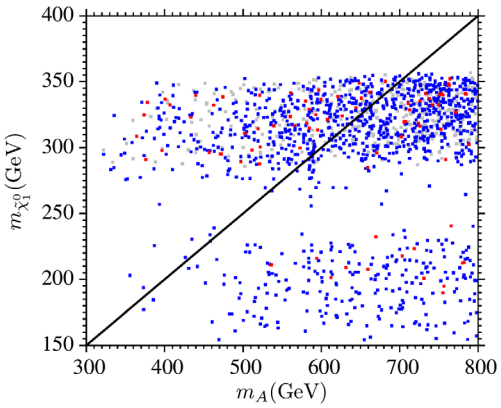

FIG. 6 (color online). Plot in the $m_{\tilde{\chi}_1^0}$–m_A plane. The color coding is the same as in Fig. 4.

TABLE I. All the masses in this table are in units of GeV. All the points satisfy the constraints described in Sec. III. Points 1 and 2 display the solutions with the minimal values of $\Delta_{\rm EW}$, which are, respectively, not consistent and consistent with the 5σ WMAP9 bounds. Point 2 is an example of Z-pole solutions. Point 3 represents a solution with large contribution to Δa_μ and consistent with the 5σ WMAP9 bounds. Point 4 and 5 are the examples with large gluino masses and 125 GeV light CP-even Higgs boson mass, which are, respectively, consistent and not consistent with the 5σ WMAP9 bounds. Points 3 and 4 are the bino-wino coannihilation scenario, while point 5 represents winolike LSP solutions.

	Point 1	Point 2	Point 3	Point 4	Point 5
$m_{\tilde{Q}}$	1268.4	1435.2	2141	2095.2	467.95
$m_{\tilde{U}^c}$	1632.2	1914.5	3022.7	2872.3	161.02
$m_{\tilde{D}^c}$	1736.7	1988.1	3004.9	2899.4	349.3
$m_{\tilde{L}}$	159.6	152.9	438.2	543.7	517.6
$m_{\tilde{E}^c}$	743.9	673.7	175.6	728.1	641.9
M_1	108.9	112.1	515	899.8	786.1
M_2	706.1	682.4	287.1	495.6	158.5
M_3	−786.9	−743.35	856.85	1506.1	1727.5
$A_t = A_b$	3564	3725	−5073	−5897	−4817
$A_{\tilde{\tau}}$	−496.7	−465.7	168.7	396.1	−250.6
$\tan\beta$	15.9	17.9	25.9	28.6	31.2
m_{H_u}	2457	2581	3160	2306	1856
m_{H_d}	2507	2523	562.6	265.9	288.8
μ	162	207	1572	3070	2553
$\Delta_{\rm EW}$	16.5	25	598	2269	1569
$\Delta_{\rm HS}$	1462	1616	3005	3540	2393
Δa_μ	11.62×10^{-10}	15.12×10^{-10}	22.40×10^{-10}	7.78×10^{-10}	11.67×10^{-10}
m_h	123	123	124	125	125
m_H	2446	2407	708	2524	2081
m_A	2430	2391	703	2507	2068
$m_{H^\pm}$	2447	2408	713	2525	2083
$m_{\tilde{\chi}^0_{1,2}}$	46, 165	48, 208	218, 234	387, 404	108, 329
$m_{\tilde{\chi}^0_{3,4}}$	173, 611	218, 591	1571, 1574	3053, 3054	2544, 2544
$m_{\tilde{\chi}^\pm_{1,2}}$	165, 605	211, 584	234, 1570	406,3059	108, 2547
$m_{\tilde{g}}$	1829	1752	2029	3323	3672
$m_{\tilde{u}_{L,R}}$	2036, 2233	2081, 2382	2689, 3411	3491, 3986	3211, 3227
$m_{\tilde{t}_{1,2}}$	830, 1401	966, 1387	1444, 1867	2298, 2592	1862, 2515
$m_{\tilde{d}_{L,R}}$	2038, 2322	2083, 2469	2690, 3433	3492, 4036	3212, 3203
$m_{\tilde{b}_{1,2}}$	1384, 2217	1354, 2342	1533, 3176	2486, 3723	2492, 2894
$m_{\tilde{\nu}_{1,2}}$	442	367	267	497	621
$m_{\tilde{\nu}_3}$	365	240	287	502	622
$m_{\tilde{e}_{L,R}}$	457, 767	384, 755	251, 552	504, 943	644, 501
$m_{\tilde{\tau}_{1,2}}$	383, 691	266, 654	247, 571	457, 948	402, 685
$\sigma_{\rm SI}$(pb)	1.54×10^{-9}	7.14×10^{-10}	4.9×10^{-11}	8.09×10^{-13}	4.65×10^{-12}
$\sigma_{\rm SD}$(pb)	2.13×10^{-4}	7.99×10^{-5}	2.62×10^{-8}	7.91×10^{-10}	3.09×10^{-8}
$\Omega_{\rm CDM}h^2$	0.006	0.122	0.096	0.103	0.0007

couple orders of magnitude below the current bounds from the COUPP experiment. For comparison, in the bottom panel of Fig. 7, we present a plot of the (nonrescaled) Higgsino-like neutralino spin-dependent cross section $\sigma^{\rm SD}(\tilde{\chi}^0_1 p)$ vs m(Higgsino). The IceCube DeepCore and future IceCube DeepCore bounds are shown by the black solid line and black dashed line [60]. The color coding is the same as the left panel. Because the IceCube detection depends on whether the Sun has equilibrated its core abundance between capture rate and annihilation rate [61], we do not rescale our results here. It was shown in Ref. [62] that for the Sun equilibration is reached for almost all of SUSY parameter space. If this is true, then our solutions will be probed by the future IceCube DeepCore experiment. However, we are not sure whether such an equilibration can be reached if the SUSY particles are relatively heavy.

In Table I, we present five benchmark points. All the points satisfy the bounds on the sparticle and Higgs boson masses as well as the constraints from B physics and Δa_μ described in Sec. III. Points 1 and 2 are the solutions with the minimal values of $\Delta_{\rm EW}$ that are, respectively, not consistent and consistent with the WMAP9 5σ bound. Here, we see that the mass of the binolike LSP neutralino is about ∼46–48 GeV, the $m_{\tilde{\chi}^\pm_1}$ range is $\sim[165, 211]$ GeV, and the CP-even Higgs boson mass is around 123 GeV. For

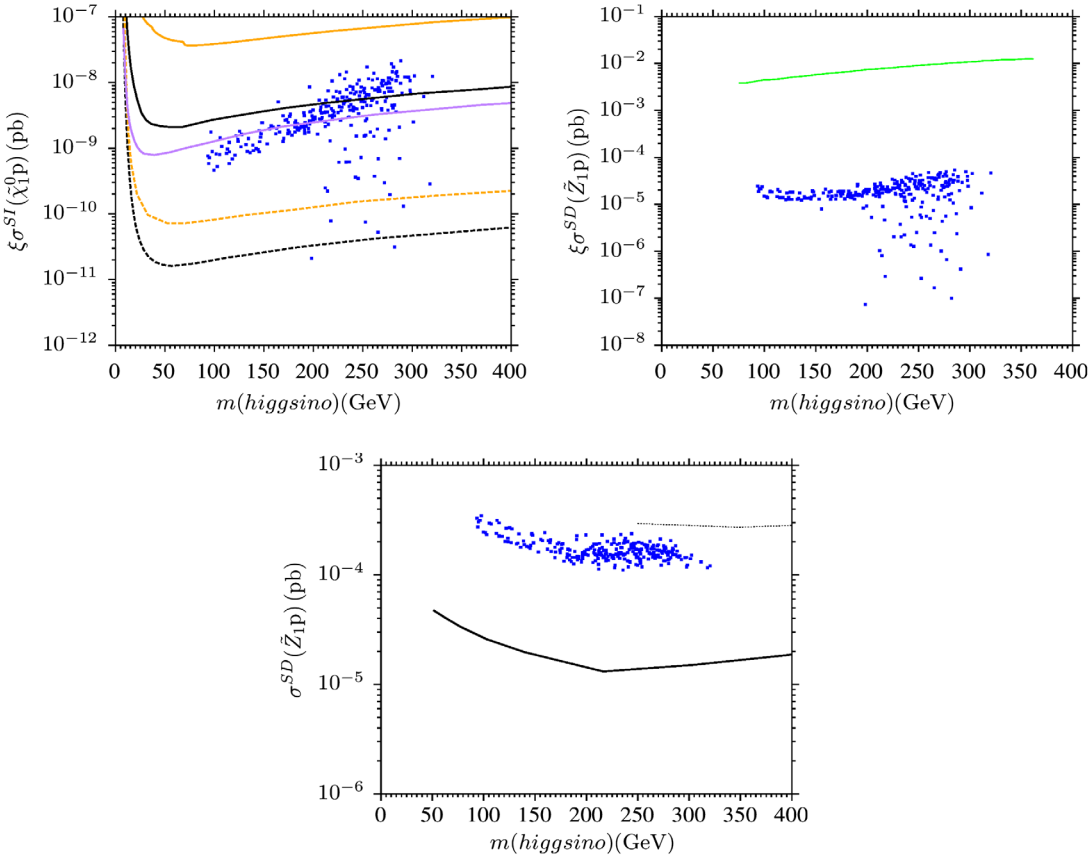

FIG. 7 (color online). In the top left panel, rescaled Higgsino-like neutralino spin-independent cross section $\xi\sigma^{\mathrm{SI}}(\tilde{\chi}_1^0 p)$ vs m(Higgsino) is shown. The orange solid line (top greyish solid line in black and white print) represents the current upper bound set by the CDMS experiment, black solid line depicts the upper bound set by XENON100 and the current upper bound set by the LUX experiment is shown by purple line (greyish solid line in black and white print), while the orange (greyish in black and white print) and black dashed lines represent, respectively, the future reach of the SuperCDMS and XENON1T experiments. The top right panel shows the plot in the rescaled Higgsino-like neutralino spin-dependent cross section $\xi\sigma^{\mathrm{SD}}(\tilde{\chi}_1^0 p) - m$(Higgsino) plane. The green line represents the upper bound set by the COUPP experiment. In the bottom panel, the (nonrescaled) Higgsino-like neutralino spin-dependent cross section $\sigma^{\mathrm{SD}}(\tilde{\chi}_1^0 p)$ vs m(Higgsino) is displayed. The IceCube DeepCore (black solid line) bound is shown, and the future IceCube DeepCore bound is depicted by the black dashed line. The color coding is the same as in Fig. 4.

the first two-family sleptons and sneutrinos, the left-handed sleptons are lighter than the right-handed sleptons and are in the mass range [380, 460] GeV, while the third-family light stau and tau sneutrino can be as light as 266 and 240 GeV, respectively. For the colored sparticles, the gluino mass is around 1800 GeV, the first two-family squarks are in the mass range ∼[2000, 2400] GeV, and the light stop is around 830 GeV. Point 2 also represents the Z-pole solutions. Point 3 represents a solution with large contribution to $\Delta a_\mu \sim 22.4 \times 10^{-10}$ (within one σ bound on Δa_μ) and consistent with the 5σ WMAP9 bounds. It is also an example of the bino-wino coannihilation scenario with $m_{\tilde{\chi}_1^0} \sim 218$ and $m_{\tilde{\chi}_1^\pm} \sim 234$ GeV. Here, we see that the Higgs boson mass is around 124 GeV; the first two families of left- and right-handed sleptons, respectively, have masses ∼251 and 552 GeV; the light stau mass is around 247 GeV; and the tau sneutrino mass is 287 GeV. The gluino mass is around 2000 GeV, while the first two families of squark masses are from 2680 to 3430 GeV. The light stop mass is around 1444 GeV. Points 4 and 5, respectively, are the examples of solutions with large gluino masses about 3323 and 4215 GeV and 125 GeV light CP-even Higgs boson mass. Point 4 is consistent with relic density bounds with $\Delta a_\mu \sim 7.87 \times 10^{-10}$, while point 5 has $\Delta a_\mu \sim 11.54 \times 10^{-10}$ but does not satisfy the relic density bound. Point 4 is another example of the bino-wino coannihilation scenario. Point 5 is representative of the winolike LSP neutralino solutions. For points 4 and 5, the first two families of right-handed sleptons are, respectively, 943 and 870 GeV, but the corresponding left-handed sleptons are 504 and 477 GeV. Also, sneutrinos have masses 497 and 430 GeV, respectively. The light stau and tau sneutrino masses for point 4 are 457 and 502 GeV, while for point 5 the light stau mass is 136 GeV, and the tau sneutrino mass is about 283 GeV.

In Table II, we display another five benchmark points consistent with the constraints described in Sec. III. Points 1, 2, 3, and 4 represent the Higgs resonance, A resonance, neutralino-stau solution, and neutralino-tau sneutrino

TABLE II. All the masses in this table are in units of GeV. All points satisfy all the constraints in Sec. III except point 4, which does not satisfy the 5σ WMAP9 bounds. Points 1, 2, 3, and 4 represent the Higgs resonance, A resonance, neutralino-stau coannihilation, and neutralino-stau neutrino coannihilation solutions, respectively. Point 5 is an example of the Higgsino-like LSP. This point has the rescaled Higgsino-like neutralino spin-independent cross section $\xi\sigma^{\rm SI}(\tilde{Z}_1 p)$ below the XENON1T experimental upper bound ($\Omega_{\tilde{\chi}_1^0}h^2/0.11 \times \sigma^{\rm SI}(\tilde{\chi}_1^0 p) \sim 2.09 \times 10^{-11}$ pb).

	Point 1	Point 2	Point 3	Point 4	Point 5
$m_{\tilde{Q}}$	1631.4	2305.6	2328.6	2344	2084.3
$m_{\tilde{U}^c}$	2302.7	3230.9	3258.8	3288.9	2907.8
$m_{\tilde{D}^c}$	2274	3246.1	3277.2	3301.6	2928
$m_{\tilde{L}}$	466.8	211.7	210.2	215.1	237.8
$m_{\tilde{E}^c}$	143.6	439.5	473.7	414	483.4
M_1	135.4	709.5	768.2	761.2	789.7
M_2	658.8	687.4	742.5	701.0	707.2
M_3	−649.7	742.65	806.75	851.5	913.45
$A_t = A_b$	4095	−4616	−4675	−4695	−4078
$A_{\tilde{\tau}}$	−202.5	918	807.3	846.7	784.8
$\tan\beta$	21.5	14.2	15.9	14.7	16.1
m_{H_u}	2708	3641	3295	3521	3472
m_{H_d}	2722	828.3	954.6	980.1	861
μ	451	503	1459	1170	209
$\Delta_{\rm EW}$	49	76	512	329	102
$\Delta_{\rm HS}$	1818	3260	3128	3318	2914
Δa_μ	12.2×10^{-10}	7.5×10^{-10}	5.76×10^{-10}	6.0×10^{-10}	10.3×10^{-10}
m_h	123	123	123	123	123
m_H	2503	577	1499	1275	401
m_A	2487	573	1490	1267	398
$m_{H^\pm}$	2504	582	1502	1278	409
$m_{\tilde{\chi}_{1,2}^0}$	60, 433	300, 478	331, 611	327, 573	198, 219
$m_{\tilde{\chi}_{3,4}^0}$	462, 586	513, 604	1466, 1469	1179, 1184	344, 589
$m_{\tilde{\chi}_{1,2}^\pm}$	440, 580	481, 598	611, 1469	573, 1184	214, 578
$m_{\tilde{g}}$	1571	1798	1933	2025	2132
$m_{\tilde{u}_{L,R}}$	2113, 2567	2715, 3515	2805, 3576	2857, 3642	2725, 3383
$m_{\tilde{t}_{1,2}}$	1034,1323	1544, 1868	1726, 2062	1741, 2064	1648, 1914
$m_{\tilde{d}_{L,R}}$	2114, 2632	2716, 3544	2806, 3625	2858, 3608	2726, 3401
$m_{\tilde{b}_{1,2}}$	1222, 2444	1631, 3453	1813, 3516	1832, 3582	1766, 3295
$m_{\tilde{\nu}_{1,2}}$	378	400	358	350	489
$m_{\tilde{\nu}_3}$	166	385	336	330	474
$m_{\tilde{e}_{L,R}}$	387, 689	399, 582	352, 731	345, 662	493, 564
$m_{\tilde{\tau}_{1,2}}$	184, 498	395, 582	340, 715	337, 646	485, 546
$\sigma_{\rm SI}$(pb)	7.42×10^{-11}	2.7×10^{-9}	1.7×10^{-11}	4.11×10^{-11}	4.66×10^{-8}
$\sigma_{\rm SD}$(pb)	3.44×10^{-6}	5.82×10^{-6}	2.82×10^{-8}	8.06×10^{-8}	1.64×10^{-4}
$\Omega_{\rm CDM}h^2$	0.129	0.098	0.124	0.123	4.94×10^{-5}

solution, respectively. Point 5 is an example of the Higgsino-like LSP. Here, we see that all of these points have a lot of common features. Gluino masses are in the range [1700, 2100] GeV, while the first two families of squarks have masses from around 2700 to 3600 GeV. The light stop mass lies in the range [1000, 1750] GeV. Also, the first two families of sleptons and sneutrinos are almost degenerate. In both tables of benchmark points, the light stop is the lightest colored sparticle. Point 5 has the rescaled Higgsino-like neutralino spin-independent cross section $\xi\sigma^{\rm SI}(\tilde{\chi}_1^0 p) = \Omega_{\tilde{\chi}_1^0}h^2/0.11 \times \sigma^{\rm SI}(\tilde{\chi}_1^0 p) \sim 2.09 \times 10^{-11}$ pb, which is below the XENON1T experimental low bound.

V. DISCUSSIONS AND CONCLUSION

We attempted to resolve the muon $(g-2)_\mu/2$ discrepancy in the SM by exploring the MSSM with the EWSUSY from GmSUGRA. We identified a viable parameter space that resolves this discrepancy, and as a by product, we obtained the solutions with small EWFT simultaneously. Our solutions not only provide sizable contributions to Δa_μ but also satisfy all the current experimental constraints including the LHC SUSY searches. In particular, the relic density for cold dark matter can be achieved within the 5σ WMAP9 bounds by the bino-wino, neutralino-stau, and neutralino-tau sneutrino coannihilation scenarios, and the A, Higgs, and Z resonance scenarios. Moreover, we identified the Higgsino-like LSP neutralino and calculate

the spin-independent and spin-dependent cross sections on the LSP neutralinos with nucleons.

ACKNOWLEDGEMENTS

We would like to thank Howard Baer for useful discussions. This research was supported in part by the Natural Science Foundation of China under Grants No. 10821504, No. 11075194, No. 11135003, No. 11275246, and No. 11475238, and by the National Basic Research Program of China (973 Program) under Grant No. 2010CB833000 (T. L.).

[1] G. Aad *et al.* (ATLAS Collaboration), Phys. Lett. B **716**, 1 (2012).
[2] S. Chatrchyan *et al.* (CMS Collaboration), Phys. Lett. B **716**, 30 (2012).
[3] S. Chatrchyan *et al.* (CMS Collaboration), Phys. Lett. B **725**, 243 (2013).
[4] G. Aad *et al.* (ATLAS Collaboration), J. High Energy Phys. 09 (2014) 176.
[5] https://twiki.cern.ch/twiki/bin/view/AtlasPublic/HiggsPublicResults; https://twiki.cern.ch/twiki/bin/view/CMSPublic/PhysicsResultsHIG.
[6] https://twiki.cern.ch/twiki/bin/view/AtlasPublic/SupersymmetryPublicResults; https://twiki.cern.ch/twiki/bin/view/CMSPublic/PhysicsResultsSUS.
[7] R. Aaij *et al.* (LHCb Collaboration), Phys. Rev. Lett. **110**, 021801 (2013).
[8] O. Buchmueller, R. Cavanaugh, A. De Roeck, J. R. Ellis, H. Flacher, S. Heinemeyer, G. Isidori, K. A. Olive, F. J. Ronga, and G. Weiglein, Eur. Phys. J. C **64**, 391 (2009).
[9] E. Barberio *et al.* (Heavy Flavor Averaging Group (HFAG) Collaboration), arXiv:0704.3575.
[10] D. Asner *et al.* (Heavy Flavor Averaging Group Collaboration), arXiv:1010.1589.
[11] Y. Amhis *et al.* (Heavy Flavor Averaging Group Collaboration), arXiv:1207.1158.
[12] M. Davier, A. Hoecker, B. Malaescu, and Z. Zhang, Eur. Phys. J. C **71**, 1515 (2011); **72**, 1874(E) (2012); K. Hagiwara, R. Liao, A. D. Martin, D. Nomura, and T. Teubner, J. Phys. G **38**, 085003 (2011).
[13] G. W. Bennett *et al.* (Muon G-2 Collaboration), Phys. Rev. D **73**, 072003 (2006); G. W. Bennett *et al.* (Muon (g-2) Collaboration), Phys. Rev. D **80**, 052008 (2009).
[14] G. Hinshaw *et al.* (WMAP Collaboration), Astrophys. J. Suppl. Ser. **208**, 19 (2013).
[15] D. S. Akerib *et al.* (LUX Collaboration), Phys. Rev. Lett. **112**, 091303 (2014).
[16] T. Cheng, J. Li, T. Li, D. V. Nanopoulos, and C. Tong, Eur. Phys. J. C **73**, 2322 (2013).
[17] T. Li and D. V. Nanopoulos, Phys. Lett. B **692**, 121 (2010).
[18] C. Balazs, T. Li, D. V. Nanopoulos, and F. Wang, J. High Energy Phys. 09 (2010) 003.
[19] T. Moroi, Phys. Rev. D **53**, 6565 (1996); **56**, 4424(E) (1997).
[20] G. Venanzoni (Fermilab E989 Collaboration), arXiv:1411.2555.
[21] M. Badziak, Z. Lalak, M. Lewicki, M. Olechowski, and S. Pokorski, arXiv:1411.1450; S. Iwamoto, T. T. Yanagida, and N. Yokozaki, arXiv:1407.4226; K. S. Babu, I. Gogoladze, Q. Shafi, and C. S. Un, arXiv:1406.6965; S. P. Das, M. Guchait, and D. P. Roy, arXiv:1406.6925; A. Freitas, J. Lykken, S. Kell, and S. Westhoff, J. High Energy Phys. 05 (2014) 145; M. A. Ajaib, I. Gogoladze, Q. Shafi, and C. S. Un, J. High Energy Phys. 05 (2014) 079; M. Endo, K. Hamaguchi, T. Kitahara, and T. Yoshinaga, J. High Energy Phys. 11 (2013) 013; N. Okada, S. Raza, and Q. Shafi, Phys. Rev. D **90**, 015020 (2014); R. Dermisek and A. Raval, Phys. Rev. D **88**, 013017 (2013); S. Akula and P. Nath, Phys. Rev. D **87**, 115022 (2013); M. Ibe, T. T. Yanagida, and N. Yokozaki, J. High Energy Phys. 08 (2013) 067; S. Mohanty, S. Rao, and D. P. Roy, J. High Energy Phys. 09 (2013) 027; T. Cheng and T. Li, Phys. Rev. D **88**, 015031 (2013); S. Iwamoto, AIP Conf. Proc. **1467**, 57 (2012).
[22] I. Gogoladze, F. Nasir, Q. Shafi, and C. S. Un, Phys. Rev. D **90**, 035008 (2014).
[23] M. Endo, K. Hamaguchi, S. Iwamoto, and T. Yoshinaga, J. High Energy Phys. 01 (2014) 123.
[24] H. Baer, F. E. Paige, S. D. Protopopescu, and X. Tata, arXiv:hep-ph/0001086.
[25] H. Baer, V. Barger, P. Huang, D. Mickelson, A. Mustafayev, and X. Tata, Phys. Rev. D **87**, 035017 (2013).
[26] J. Hisano, H. Murayama, and T. Yanagida, Nucl. Phys. **B402**, 46 (1993); Y. Yamada, Z. Phys. C **60**, 83 (1993); J. L. Chkareuli and I. G. Gogoladze, Phys. Rev. D **58**, 055011 (1998).
[27] D. M. Pierce, J. A. Bagger, K. T. Matchev, and R.-j. Zhang, Nucl. Phys. **B491**, 3 (1997).
[28] L. E. Ibanez and G. G. Ross, Phys. Lett. B **110**, 215 (1982); K. Inoue, A. Kakuto, H. Komatsu, and S. Takeshita, Prog. Theor. Phys. **68**, 927 (1982).**70**, 330 (1983); L. E. Ibanez, Phys. Lett. B **118**, 73 (1982); J. R. Ellis, D. V. Nanopoulos, and K. Tamvakis, Phys. Lett. B **121**, 123 (1983); L. Alvarez-Gaume, J. Polchinski, and M. B. Wise, Nucl. Phys. **B221**, 495 (1983).
[29] J. Beringer *et al.* (Particle Data Group Collaboration), Phys. Rev. D **86**, 010001 (2012).
[30] Tevatron Electroweak Working Group and CDF Collaboration and D0 Collab, arXiv:0903.2503.
[31] I. Gogoladze, R. Khalid, S. Raza, and Q. Shafi, J. High Energy Phys. 06 (2011) 117.
[32] G. Belanger, F. Boudjema, A. Pukhov, and R. K. Singh, J. High Energy Phys. 11 (2009) 026; H. Baer, S. Kraml, S. Sekmen, and H. Summy, J. High Energy Phys. 03 (2008) 056.
[33] H. Baer and M. Brhlik, Phys. Rev. D **55**, 4463 (1997); H. Baer, M. Brhlik, D. Castano, and X. Tata, Phys. Rev. D **58**, 015007 (1998);

[34] K. Babu and C. Kolda, Phys. Rev. Lett. **84**, 228 (2000); A. Dedes, H. Dreiner, and U. Nierste, Phys. Rev. Lett. **87**, 251804 (2001); J. K. Mizukoshi, X. Tata, and Y. Wang, Phys. Rev. D **66**, 115003 (2002).
[35] D. Eriksson, F. Mahmoudi, and O. Stal, J. High Energy Phys. 11 (2008) 035.
[36] R. Rattazzi and U. Sarid, Nucl. Phys. **B501**, 297 (1997).
[37] J. Hisano and S. Sugiyama, Phys. Lett. B **696**, 92 (2011); **719**, 472 (2013).
[38] R. Sato, K. Tobioka, and N. Yokozaki, Phys. Lett. B **716**, 441 (2012); T. Kitahara and T. Yoshinaga, J. High Energy Phys. 05 (2013) 035; M. Carena, S. Gori, N. R. Shah, C. E. M. Wagner, and L. T. Wang, J. High Energy Phys. 08 (2013) 087.
[39] G. Aad *et al.* (ATLAS Collaboration), J. High Energy Phys. 04 (2014) 169.
[40] G. Aad *et al.* (ATLAS Collaboration), J. High Energy Phys. 05 (2014) 071.
[41] CMS Collaboration, Report No. CMS-PAS-SUS-13-006.
[42] CMS Collaboration, Report No. CMS-NOTE-2012-006.
[43] H. Baer, M. Berggren, J. List, M. M. Nojiri, M. Perelstein, A. Pierce, W. Porod, and T. Tanabe, arXiv:1307.5248.
[44] H. Baer *et al.*, arXiv:1306.6352.
[45] S. Schael *et al.* (ALEPH Collaboration, DELPHI Collaboration, L3 Collaboration, OPAL Collaboration, SLD Collaboration, LEP Electroweak Working Group, SLD Electroweak Group, SLD Heavy Flavour Group Collaboration), Phys. Rep. **427**, 257 (2006).
[46] T. Han, Z. Liu, and S. Su, J. High Energy Phys. 08 (2014) 093.
[47] G. Belanger, B. Dumont, U. Ellwanger, J. F. Gunion, and S. Kraml, Phys. Lett. B **723**, 340 (2013).
[48] R. Peccei and H. Quinn, Phys. Rev. Lett. **38**, 1440 (1977); Phys. Rev. D **16**, 1791 (1977); S. Weinberg, Phys. Rev. Lett. **40**, 223 (1978); F. Wilczek, Phys. Rev. Lett. **40**, 279 (1978); Nucl. Phys. **B198**, 102 (1982); J. E. Kim, Phys. Lett. **136B**, 378 (1984); J. E. Kim and H. P. Nilles, Phys. Lett. **138B**, 150 (1984); for a review, see, e.g., F. D. Steffen, Eur. Phys. J. C **59**, 557 (2009); H. Baer, M. Haider, S. Kraml, S. Sekmen, and H. Summy, J. Cosmol. Astropart. Phys. 02 (2009) 002; Phys. Rev. Lett. **82**, 4180 (1999); L. Covi, H. B. Kim, J. E. Kim, and L. Roszkowski, J. High Energy Phys. 05 (2001) 033.
[49] K.-Y. Choi, J. E. Kim, H. M. Lee, and O. Seto, Phys. Rev. D **77**, 123501 (2008); H. Baer, S. Kraml, A. Lessa, and S. Sekmen, J. Cosmol. Astropart. Phys. 04 (2011) 039; H. Baer and A. Lessa, J. High Energy Phys. 06 (2011) 027; H. Baer, A. Lessa, S. Rajagopalan, and W. Sreethawong, J. Cosmol. Astropart. Phys. 06 (2011) 031; H. Baer, A. Lessa, and W. Sreethawong, J. Cosmol. Astropart. Phys. 01 (2012) 036.
[50] J. Fan and M. Reece, J. High Energy Phys. 10 (2013) 124.
[51] T. Cohen, M. Lisanti, A. Pierce, and T. R. Slatyer, J. Cosmol. Astropart. Phys. 10 (2013) 061.
[52] A. Hryczuk, I. Cholis, R. Iengo, M. Tavakoli, and P. Ullio, J. Cosmol. Astropart. Phys. 07 (2014) 031.
[53] L. F. Abbott and P. Sikivie, Phys. Lett. **120B**, 133 (1983); J. Preskill, M. Wise, and F. Wilczek, Phys. Lett. **120B**, 127 (1983); M. Dine and W. Fischler, Phys. Lett. **120B**, 137 (1983); M. Turner, Phys. Rev. D **33**, 889 (1986); L. Visinelli and P. Gondolo, Phys. Rev. D **80**, 035024 (2009).
[54] E. Aprile *et al.* (XENON100 Collaboration), Phys. Rev. Lett. **109**, 181301 (2012).
[55] P. L. Brink *et al.* (CDMS-II Collaboration), Beyond the CDMS-II dark matter search: SuperCDMS, eConf C041213, 2529 (2004).
[56] E. Aprile (XENON1T Collaboration), Springer Proc. Phys. **148**, 93 (2013).
[57] A. Bottino, F. Donato, N. Fornengo, and S. Scopel, Phys. Rev. D **63**, 125003 (2001).
[58] H. Baer, V. Barger, and D. Mickelson, Phys. Lett. B **726**, 330 (2013).
[59] E. Behnke *et al.* (COUPP Collaboration), Phys. Rev. D **86**, 052001 (2012).
[60] R. Abbasi *et al.* (ICECUBE Collaboration), Phys. Rev. Lett. **102**, 201302 (2009).
[61] G. Jungman, M. Kamionkowski, and K. Griest, Phys. Rep. **267**, 195 (1996).
[62] V. Niro, A. Bottino, N. Fornengo, and S. Scopel, Phys. Rev. D **80**, 095019 (2009).